





# Physicochemical and Biopharmaceutical Controllability of New Self-Assembled Fatty Acid Conjugated Leuprolide for the Enhanced Anticancer Activity

Hai V Ngo <sup>1</sup>, Hye-Eun Bak<sup>1</sup>, Hy D Nguyen <sup>1</sup>, Kye Wan Lee<sup>2</sup>, Chulhun Park <sup>3</sup>, Beom-Jin Lee <sup>1</sup>

<sup>1</sup>College of Pharmacy, Ajou University, Suwon, 16499 Republic of Korea; <sup>2</sup>Dongkook Pharmaceutical Co., Ltd., Seoul, 06072 Republic of Korea;

<sup>3</sup>College of Pharmacy, Jeju National University, Jeju, 63243 Republic of Korea

Correspondence: Beom-Jin Lee, College of Pharmacy, Ajou University, Suwon, 16499, Republic of Korea, Email [bjl@ajou.ac.kr](mailto:bjl@ajou.ac.kr)

**Background:** Leuprolide (LEU), a synthetic nonapeptide analog of naturally occurring gonadotropin-releasing hormone (GnRH), could exert a direct inhibitory activity on the proliferation of prostate cancer cells. However, the short half-life in blood and the biopharmaceutical problem of LEU limit this anticancer activity.

**Purpose:** To improve its druggability for improving anticancer activity, the amine-group targeted LEU was conjugated with different chain lengths of saturated fatty acids (FAs).

**Methods:** LEU–fatty acid conjugates (LFCs) were synthesized by exploiting N-hydroxysuccinimidyl (NHS) conjugation chemistry. The physicochemical properties and the self-assembled behaviors of the conjugates were extensively investigated. The in vitro anticancer activity of three LFCs was extensively studied in both 2D monolayer and 3D spheroid culture models of a prostate cancer cell line, PC3.

**Results:** Three LFCs could be readily self-assembled into nanoparticles (LFNs) with a small size of around 100 nm, positive charges, and exhibited greater permeability rates compared to the same concentration of LEU, excluding LSN. The chain length of FA in conjugate was positively related to the selectivity index between cancer cells and non-cancerous cell lines. All LFCs showed a superior direct antiproliferative effect on cancer cells in the following order: LSC (98.9%) > LPC (86.7%) > LLC (75.0%) > LEU (8.9%) after repeat daily of the same dose strength of LEU for 4 days. In addition, the 3D spheroid model study indicates that all LFCs with a one-time treatment performed a long-acting inhibitory effect on tumor growth as compared to LEU after 7 days.

**Conclusion:** The conjugation of LEU with different chain lengths of FAs could provide a novel strategy to improve peptide stability and exert an additional superior direct inhibitory effect for the treatment of several hormone-responsive tumor systems using therapeutic peptides.

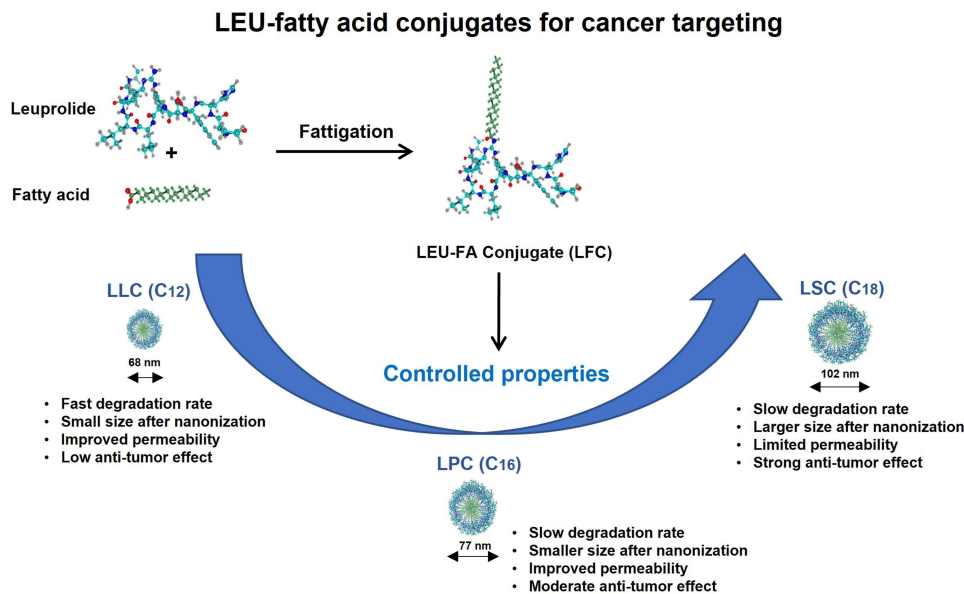
**Keywords:** leuprolide, fattigation, fatty acid chain length, LEU–fatty acid conjugate, self-assembled nanoparticles, enhanced permeability, improved anticancer activity

## Introduction

Prostate cancer has become the leading common primary cancer as a cause of cancer-related illness and death in men.<sup>1,2</sup> The prevention and treatment of different stages of prostate cancer can be achieved by several options including radiation therapy, immunotherapy, cryotherapy, chemotherapy, and hormone therapy.<sup>2,3</sup> Among them, hormone therapy, also called androgen suppression therapy, has been considered as the standard first-line treatment for metastatic prostate cancer by lowering levels of male hormones (androgens) as fuels for prostate cancer cell growth.<sup>4,5</sup>

Leuprolide (LEU) acetate, a synthetic nonapeptide and a potent GnRH agonist that lowers gonadotropin secretion, has been used as the first-line treatment for advanced prostate cancer.<sup>6</sup> Unfortunately, like other peptide drugs, LEU has many biopharmaceutical limitations such as a short half-life and low membrane permeability. Table 1 gives the physicochemical

Graphical Abstract



and biological properties of LEU. For these reasons, various pharmaceutical technologies have been utilized to encapsulate and deliver LEU acetate for long-acting injection.<sup>7,8</sup> For example, PLGA microspheres encapsulating LEU were developed for parenteral controlled release depot injection.<sup>9</sup> In situ forming implant (ISFI) system using PLGA and nanohydroxyapatite (HA) particle also led to the sustained release of LEU and testosterone withholding over a 90-day period with a significant decrease in the burst release phase.<sup>10</sup> Currently, LEU depot suspension (Lupron Depot<sup>®</sup>, TAP Pharmaceuticals Inc., Deerfield, IL, USA) is commercially available in a prefilled dual-chamber syringe containing sterile lyophilized microspheres, which is administered monthly as an intramuscular (IM) injection with sustained release.<sup>11</sup>

Recent advances both in vitro and in vivo indicate that many GnRH agonists, including LEU, exert direct inhibitory effects on tumor growth on various cancer cell lines containing both androgen-dependent and androgen-independent models by interfering with the pro-metastatic activity of insulin-like growth factor-I (IGF-1) and resulting in the reduced migration.<sup>12–15</sup> However, the magnitude of this effect at doses was insufficient due to the short serum half-life and unmet biopharmaceutical and physicochemical properties of LEU, thereby cell proliferation studies were performed by daily treatment of LEU to clearly exert the significant inhibitory effect on the migration and invasion of androgen-independent

**Table I** Physicochemical and Biological Properties of Leuprolide (LEU) Acetate

Factor	Leuprolide Acetate
Physical appearance	White solid
Molecular weight	1269.5 g/mol
Chemical formula	C <sub>61</sub> H <sub>88</sub> N <sub>16</sub> O <sub>14</sub> · C <sub>2</sub> H <sub>4</sub> O <sub>2</sub>
Half-life	3 h
Drug class	GnRH analogue; GnRH agonist
Route of administration	IM injection
Excretion	Kidney
Solubility in water	Highly water-soluble, ≥ 66.66 mg/mL
Log P	-2.7
Physiological charge	+1

prostate cancer cells.<sup>12</sup> Lipidation is a promising strategy to modulate the lipophilicity, secondary structures, and self-assembly of various proteins and peptides by the presence of a lipid group after conjugation.<sup>16</sup> These modifications could be useful for improving metabolic stability, membrane permeation, and modulating the pharmacokinetic as well as pharmacodynamic properties of peptides.<sup>17</sup> Among many strategies of using lipid groups in lipidation, the fattigation-platform technology developed by our research group can be a superior alternative to modify and improve the druggability of various peptide and protein medicines by utilizing diverse characteristics of fatty acids.<sup>18,19</sup> There are two properties of fatty acids making them different from one another, including carbon chain length and degree of saturation.<sup>19</sup> In the previous study, our group investigated the importance of fatty chain length in *in vitro* and *in vivo* of anticancer activity in many cancer cell lines and suggested that the long -chain fatty acids could have the potential for cancer targeting due to the overexpression of free-fatty acid receptors (FFARs) on cancer cells.<sup>20–22</sup> Recently, we synthesized and studied the modifications of the hydroxy group-targeted conjugates of LEU with different degrees of saturation of fatty acids affecting the improved kinetic peptide degradation against human plasma and the enhanced permeability through self-assembled nanoparticles of these conjugates.<sup>19</sup> In this research, the motivations come up with previous studies of our group by focusing on the importance of fatty chain lengths on the improved druggability of LEU for anticancer activity, including a long-acting performance via the enhanced drug stability and permeability, and a synergistic direct inhibitory effect with conjugated fatty acids. Amphiphilic LEU–fatty acid conjugates (LFCs) were synthesized using the N-hydroxysuccinimidyl (NHS) conjugation chemistry reaction. The physicochemical properties of the conjugates were successfully identified by <sup>1</sup>H-nuclear magnetic resonance (1H-NMR) spectroscopy, Fourier-transform infrared (FT-IR) spectroscopy, and matrix-assisted laser desorption/ionization-time-of-flight/time-of-flight (MALDI-TOF/TOF) tandem mass spectrometry. The physicochemical properties, such as particle size, surface charge, secondary structure, and morphology of LFNs, were characterized. The *in vitro* release rate of active LEU was examined using various LFC formulations after incubation with human plasma (pH 7.4) at 37 °C. In addition, the permeation test of LFNs through the cellulose membrane was carried out using a Franz diffusion cell to perceive the enhanced permeability. Finally, we examined the direct antiproliferative effect of three LFCs on the PC3 cell line. PC3 is a hormone-insensitive prostate cancer cell line and PCa is reported as a lipid-dependent tumor;<sup>23</sup> therefore it would be clearer to understand the impacts of conjugated fatty acids on the direct inhibitory effects of LFNs as compared to that of LEU. Together with 2D cell cultures, a three-dimensional (3D) spheroid culture assay was performed in this study mimicking solid tumors to observe and understand the anticancer activity of LFNs. In the meantime, we also investigated the selective toxicity to cancer cells over non-cancerous cell lines (human fibroblasts) to observe the impacts of chain length on the selectivity index of three conjugates.<sup>24</sup>

## Materials and Methods

### Materials

LEU acetate was purchased from Anygen (Gwangju, Korea). Palmitic acid N-hydroxysuccinimide ester (PA), stearic acid N-hydroxysuccinimide ester (SA), lauric acid N-hydroxysuccinimide ester (LA), sodium stearate, sodium palmitate, and sodium dodecanoate were purchased from Sigma-Aldrich. Human plasma was kindly donated from the Seoul Clinical Laboratories (Suwon, Korea). Tetrahydrofuran (THF) and dimethyl sulfoxide (DMSO) were obtained from Daejung Chemicals & Metals (Seoul, Korea). HPLC-grade solvents were obtained from Thermo Fisher Scientific with anhydrous alcohol (EtOH), methanol (MeOH), acetonitrile (ACN), Tween<sup>®</sup> 80, and formic acid (Asheville, NC, USA). All other reagents were of analytical grade and used commercially without purification.

### Preparation of LFCs

#### Screening Fatty Acid Agents

LFCs were synthesized by exploiting the NHS conjugation chemistry reaction to target the amine groups. For example, the scheme of the LEU–palmitic acid NHS ester coupling reaction for the conjugation process is shown in [Figure 1](#). Fatty acids were chosen as the backbone of the conjugates, based on a previous study. Different saturated fatty acid NHS esters were selected, namely, lauric acid-NHS ester (NHS-LA) (C12), palmitic acid-NHS ester (NHS-PA) (C16), and stearic acid-NHS ester (NHS-SA) (C18). The physicochemical properties of the selected fatty acids are summarized in [Table 2](#).

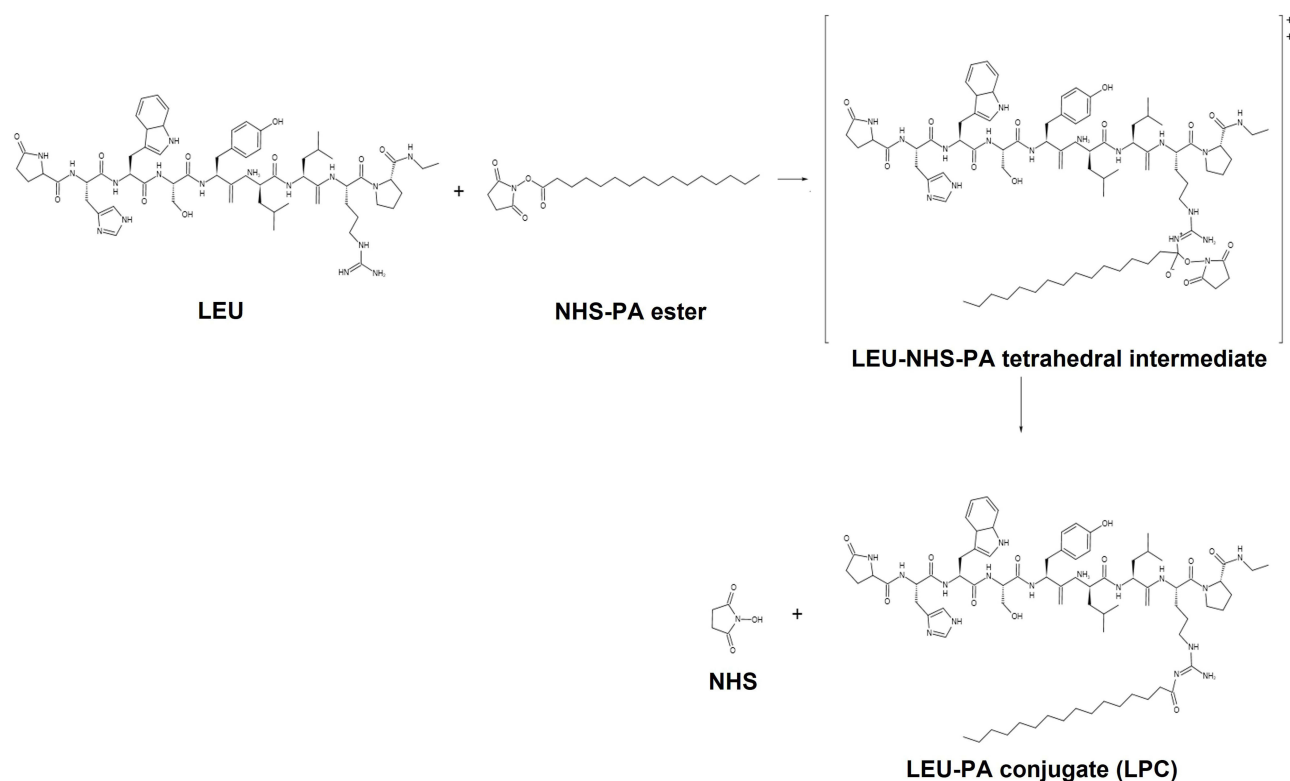


**Figure 1** Schematic diagram for the synthesis of amine-group targeted LEU–palmitic acid conjugate (LPC).

## Synthesis of LFCs

LFCs were synthesized using the NHS conjugation chemistry reaction, as described previously with some modifications.<sup>25,26</sup> Briefly, 127 mg (0.1 mM) of LEU acetate was dissolved in 10 mL of pH 7.4 phosphate-buffered saline (PBS) solution under stirring at 500 rpm for 3 h to deprotonate the Arg guanidinium group of LEU, therefore promoting the nucleophilic attack of the activated esters at room temperature. At the same time, 35.35 mg (0.1 mM) of NHS-PA was dissolved in 10 mL of THF (the synthesis of other types of fatty acids (FA) was also the same mole ratio). Then, the NHS-PA solution was slowly dropped into the free-LEU solution and mixed by stirring at 500 rpm at 50 °C for 6 h to form the LPC. After the reaction, the solution was dialyzed against absolute ethanol (1000 Da MWCO) for 1 day and deionized water for 1 day to remove the residual acetate salt and organic solvents. Finally, the crude LFC solution was lyophilized at –80 °C to collect the powders.

## Purification of LFCs

To identify LEU and three types of conjugates (LFCs), they were first investigated by reverse-phase (RP) preparative HPLC separately due to the lipophilic difference between LEU acetate and LFCs. The model was a DeltaprepLC300 by Waters. Reverse-phase preparative-HPLC with an isocratic elution was equipped with a YMC-Pack C18 column

**Table 2** Physicochemical Properties of Different Chain Lengths of Fatty Acid-NHS Esters

Types of Fatty Acid-NHS Esters	Chemical Formula	Features	Molecular Weights (g/mol)	Molecular Weights of Fatty Acids (g/mol)
LA-NHS ester (C12)	$\text{CH}_3(\text{CH}_2)_{10}\text{COOHC}_4\text{H}_3\text{NO}_2$	C12, saturated	297.39	200.32
PA-NHS ester (C16)	$\text{CH}_3(\text{CH}_2)_{14}\text{COOHC}_4\text{H}_3\text{NO}_2$	C16, saturated	353.50	256.40
SA-NHS ester (C18)	$\text{CH}_3(\text{CH}_2)_{16}\text{COOHC}_4\text{H}_3\text{NO}_2$	C18, saturated	381.55	284.48



**Table 3** Prep-HPLC Gradient Conditions for LEU–Fatty Acid Conjugate (LFC) Purification

Time (Min)	D.W (0.1% TFA)	ACN (0.1% TFA)
0	80	20
10	65	35
15	30	70
30	18	82
35	0	100
40	0	100

AA30S05-2502WT (particle size 5  $\mu\text{m}$ , pore size 30 nm, 250 $\times$ 20 mm, pressure limit 20–30 MPa) and a UV detector controlled at 220 nm to assess the purity of the LFCs.

In addition, the conjugates (LFCs) were further purified using preparative high-performance liquid chromatography (Prep-HPLC) for minimizing the impurities and finally to obtain the intended one fatty acid LEU conjugate. The HPLC profiles of LEU and its conjugates were eluted at the different retention times. Gradient elution was performed at a flow rate of 10 mL/min with mobile phase A (0.1% trifluoroacetic acid (TFA) in water) and mobile phase B (0.1% TFA in acetonitrile). The column was equilibrated and eluted under gradient conditions at a flow rate of 10 mL/min and maintained at 25  $^{\circ}\text{C}$ , as shown in Table 3. The sample injection volume was 10 mL. The LFC peak was detected at an 80% solvent B ratio (retention time of approximately 21 min) in the chromatogram. The collected sample from Prep-HPLC was solvent-free using rotary evaporation and freeze-drying at  $-80^{\circ}\text{C}$  to collect the solid forms.

## Determination and Physicochemical Characterizations of LFCs

### Matrix-Assisted Laser Desorption/Ionization (MALDI-TOF)

The molecular weights of LFCs were confirmed by MALDI-TOF/TOF MS using an Autoflex maX TOF/TOF mass spectrometer with a laser frequency of 200 Hz (Bruker Daltonics, Billerica, MA, USA).  $\alpha$ -Cyano-4-hydroxycinnamic acid (CHCA, MW 189.04 Da) matrix was chosen as the peptide calibration reagent with MW <10,000 Da. In addition, 2,5-dihydroxybenzoic acid (2,5-DHB, MW 154.03 Da) was used for our LFC analysis. After Prep-HPLC purification, the LFC sample was dissolved in 75% ACN solution, and a mixture of 2  $\mu\text{L}$  samples and 2  $\mu\text{L}$  2,5-DHB matrix was prepared in a 1:1 ratio. The sample was loaded into the template (MTP 384 target plate ground steel BC, Bruker) and then measured after drying the organic solvent with a vacuum dryer.

### Proton Nuclear Magnetic Resonance ( $^1\text{H-NMR}$ )

LEU acetate and LFCs were dissolved in deuterated DMSO (DMSO- $d_6$ ) at a concentration of 20 mg/mL.  $^1\text{H-NMR}$  spectra were analyzed using a Bruker ADVANCE II 400 MHz spectrometer at 25  $^{\circ}\text{C}$ .

### Fourier Transform-Infrared (FT-IR) Spectrometer

This method was used to confirm the conjugation between LEU acetate and different types of NHS-FA esters. LEU acetate, NHS-FA esters, physical mixtures (PMs), and LFCs powders were analyzed using a FT-IR spectrometer (Nicolet iS50, Thermo Fisher, Japan). Briefly, 1 mg of each sample was mixed with 200 mg of KBr. The compressed mixture pellet was scanned at wavelengths ranging from 400 to 2000  $\text{cm}^{-1}$  with a resolution of 2  $\text{cm}^{-1}$ .

### Differential Scanning Calorimetry (DSC)

The thermodynamic features of LEU acetate, NHS-FA esters, and LFCs were measured using DSC (GmbH-DSC 200 F3 Maia<sup>®</sup>, NETZSCH, Germany). DSC data provide the melting point and physical form (amorphous/crystalline) of the measured samples. All samples were scanned from 0  $^{\circ}\text{C}$  to 200  $^{\circ}\text{C}$  at a rate of 10  $^{\circ}\text{C}/\text{min}$ .

## Circular Dichroism (CD) Spectra

The CD spectra of LEU and LFCs were measured using a CD spectroscopy (JASCO J-1500, Japan) in the range of wavelength from 190 to 260 nm. Samples (0.5 mg/mL) were prepared in water or 50% 2,2,2-trifluoroethanol (TFE)/water (v/v). Measurements were carried out with 1 mm path cell at room temperature with the scanning speed of 200 nm/min, 0.1 nm data pitch and 1 nm bandwidth.

## HPLC Analysis

A HPLC system (Agilent 1200, Agilent Technologies, USA) was equipped with a reverse phase column (Phenomenex Gemini<sup>®</sup>, C18, 5  $\mu$ m, 250 $\times$ 4.6 mm, 110 Å). For the quantitation of LEU, the mobile phase consisted of 0.1% trifluoroacetic acid (TFA) in deionized water and acetonitrile solution at a ratio of 68:32 (v/v), with a flow rate of 1 mL/min. In the case of LFCs, the mobile phase consisted of 0.1% TFA in deionized water and acetonitrile solution at a ratio of 32:68 (v/v). However, when the quantity of LEU and LFCs after degradation and permeation tests was assayed, the analyte adsorption on the C18 phase was not sufficiently strong. Accordingly, an ion-pairing reagent was added to the mobile phase solution to enhance the analyte retention. Alkyl sulfonates are typical counterions for cationic substances. Consequently, 0.01 M sodium hexane sulfonate was added to all the mobile phases with deionized water. The analytical C18 column was maintained at  $25 \pm 0.5$  °C and the loading volume of each sample was 30  $\mu$ L. The UV detector was operated at 220 nm of wavelength. The peaks of LFCs were detected at 3.030 min, 6.184 min, and 10.416 min for LLC, LPC and LSC, respectively (the HPLC profiles of LFCs are supplied in [Figure S1](#)).

## Determination of Free Amine Groups by TNBS Method

2,4,6-Trinitrobenzene sulfonic acid (TNBS) is the reagent used to quantify the number of amine groups presented in peptides, amino acids, and proteins by forming an orange-colored complex.<sup>22</sup> In this method, L-lysine monohydrate is used as a standard amino acid to establish the calibration curve in the range of 1–10  $\mu$ g/mL (equivalent to 0.0061–0.0609 mM) with  $R^2 = 0.998$  for quantitation of free amine groups. All samples including LEU acetate and LFCs (equivalently to 0.0394 mM of LEU) were prepared in 0.5 mL of reaction buffer (0.1M sodium bicarbonate, pH 8.5) with the assistance of sonication for a homogeneous distribution, followed by the adding of 0.25 mL of 0.01% TNBS solution. Then, samples were incubated for 2 h at 37 °C. After incubation, 0.25 mL of 10% (w/v) sodium lauryl sulfate (SLS) and 0.125 mL of HCl 1N were added to each sample. Finally, 200  $\mu$ L of each sample was added into each well of a 96-well plate for the absorbance measurement at 335 nm.

## Formation and Characterization of LFCs Self-Assembly (LFNs)

### Dynamic Light Scattering (DLS) Measurement

The particle size and zeta potential of the LFNs were measured using DLS ELSZ-2000 S (Otsuka Electronics, Tokyo, Japan). First, 10 mg of each LFC were dissolved in 1 mL of absolute ethanol followed by the slowly adding of 10 mL of DW. Then, the mixture was stirred for one day to evaporate the organic solvent and obtain nanonization (LFNs).

The short-term stability of LFNs with or without supplemented 5% (w/v) human serum albumin (HSA, fatty acids free) were carried out in PBS (pH 7.4) solution.<sup>27</sup> Human plasma was replaced by human serum albumin to avoid the presence of various components in plasma affecting to the accuracy of DLS measurement. Briefly, each LFN solution was diluted 5 times with PBS solution instead of DW for DLS measurement. To mimic the physiological condition, 5% w/v HSA was added. Finally, samples were incubated at 37 °C and the particle size was monitored for 48 h. All the measurements were performed in triplicate ( $n = 3$ ).

### Field Emission-Scanning Electron Microscopy (FE-SEM)

The morphology of LEU acetate and LFNs was observed by FE-SEM, JSM-7900F (Tokyo, Japan) at a voltage of 5 kV. The LFC nanonization solutions were pre-coated with a thin layer of platinum for 10 min.

### In vitro Permeation Test of LEU and LFNs

In vitro permeation of LFN solution was carried out using a Franz diffusion cell system (DHC-6TD, Logan, USA). This cell consisted of donor and receptor parts in which the permeation barrier-membrane (PB-M, cellulose membrane, Logan, USA)

was placed. The exposed membrane surface area was  $38 \text{ mm}^2$ , and the receptor compartment volume was 5 mL. LFCs were nanonized in pH 6.8 buffer solution under the same conditions as previously mentioned in the DLS method. Briefly, 10 mg of LEU or each type of LFCs was dissolved in 1 mL of absolute ethanol, and then 10 mL of PBS (pH 6.8) was slowly injected. Nanonization was performed by stirring for one day for solvent evaporation. After cell assembly, the receptor chamber was filled with PBS (pH 7.4) containing 0.5% (v/v) Tween 80 and preheated at  $37^\circ\text{C}$  and continuously stirred at 600 rpm using a magnetic stirrer. Then, 300  $\mu\text{L}$  of each sample was placed separately on the surface of the PB-M ( $n = 3$ ). Eventually, samples were withdrawn at 500  $\mu\text{L}$  at 15, 30, 60, 120, 240, 360, 480, 600, and 720 min and replenished with 500  $\mu\text{L}$  of fresh buffer. Finally, the withdrawn samples were analyzed by HPLC, as described above.

## In vitro Cell Culture Study

### Cell Lines and Cell Culture

The human prostate cancer cell line PC3 was obtained from Korean Cell Line Bank (Seoul, Korea). Human fibroblasts (human dermal fibroblasts, HDFs and human foreskin fibroblasts, HFF-1) were purchased from ATCC (Manassas, VA, USA) and used as non-cancerous cell lines in this study. All cell lines were cultured in RPMI 1640 medium supplemented with 10% fetal bovine serum (FBS) and 1% streptomycin and penicillin (Gibco, USA) and maintained in a humidified incubator at  $37^\circ\text{C}$  with 5%  $\text{CO}_2$  in air.

### Cell Viability and Proliferation Assays in 2D Monolayer Culture Model

To study the cell viability and antiproliferative effect, all cells with different cell lines were trypsinized and seeded into 48-well plates at a density of  $1 \times 10^4$  cells/well following the previous protocol.<sup>28</sup> After 24 h of incubation, cells were treated with 500  $\mu\text{L}$  of different concentrations of LEU, FAs, mixtures of LEU and FAs, and LFCs in 2.5% FBS-RPMI 1640 medium. The cell viability and proliferation assays were performed using WST-1 and live/dead assays. At the end of the incubation period, 50  $\mu\text{L}$  of WST-1 reagent (EZ-Cytox, DoGen, Korea) was added into each well and incubated for 1 h. Afterwards, the absorbance of cell culture media was measured at 450 nm using a microplate reader (Synergy H1, Biotek™, USA). The control samples were cells incubated in 2.5% FBS-RPMI 1640 without any treatments. Notably, due to the short stability of LEU in serum, a cell proliferation assay during 96 h was performed and repeated daily for all samples.<sup>15,28</sup>

To investigate the live/dead cell performance, at the end of treatment, cultured media were withdrawn and replenished carefully with live/dead working solution prepared using the LIVE/DEAD® Viability/Cytotoxicity assay kit (Invitrogen™, Thermo Fisher Scientific, USA) and following the manufacturing protocol. Notably, the positive control (live cells) samples were the samples incubated with media without any treatments. The negative control (dead cells) samples were obtained by fixing them with ice-cold 70% ethanol for 15 mins as recommended by Cell Analysis Support Center (ThermoFisher Scientific). Images were captured by utilizing a fluorescent microscope (Leica Microsystems, Korea).

### Anti-Tumor Response in 3D Spheroid Culture Model

After cell culture, the trypsinized cells were dispersed in 10% FBS-RPMI 1640 media containing 1% (v/v) Corning Matrigel® matrix to obtain the cell suspension at the density of 2000 cells/mL. Then, 250  $\mu\text{L}$  of cell suspension was added into each well of a 96-well floater plate (ultra-low attachment, SPL Life Sciences Co., Ltd), centrifuged at 1500 rpm for 10 min and left in the incubator at  $37^\circ\text{C}$  with 5%  $\text{CO}_2$ . After 4 days, when the spheroids were formed, different samples were treated at the final concentration of 50  $\mu\text{M}$  in 2.5% FBS-RPMI 1640 media. In the case of LEU, we performed two methods of treatment, including a one-time treatment (LEU) and daily treatment (LEU-D). After 7 days, the cell culture media were carefully replaced by live/dead working solution same as in 2D monolayer cell culture and incubated for 2 h before live/dead imaging. The observation and analysis of the spheroid area were performed and quantified using Cell<sup>3</sup> iMager duos (SCREEN Holdings Co., Ltd.) and ImageJ software, respectively.<sup>29</sup> The fold increase of the spheroid area was determined by the ratio between the spheroid area of each day and the spheroid area at day 0.

### Statistical Analysis

The statistical analysis of the comparison between samples was performed using Sigmaplot software (version 14.0). The one-way analysis of variance (ANOVA) was used to run the statistical significance between different groups. Data are

presented as mean  $\pm$  standard deviation. The  $p$ -value less than 0.05 was considered to be statistically significant between these groups. IC<sub>50</sub> values were determined using GraphPad Prism 5 software (GraphPad Software, CA, USA).

## Results and Discussion

### Identification and Physicochemical Characterization of LFCs

When NHS conjugation chemistry is used for conjugation, the target site can be a nucleophilic site on the peptide. The predicted sites including the  $\alpha$ -amino group of the N-terminal residue and the  $\epsilon$ -amino groups of lysine residues were absent in the LEU structure. However, the two nucleophilic sites of LEU can still be considered as possible fattigation parts. One is the guanidino group on the arginine residue, and the other is the imidazolyl group on the histidine residue.

In this research, LEU acetate was at first dissolved in PBS (pH 7.4) to deprotonate the Arginine guanidinium group of LEU, therefore promoting the nucleophilic attack of the activated esters as mentioned previously. In addition, it was indicated that if LEU was conjugated at the His residue, the imidazole ring peak of LEU positioning at 8.23 ppm would be divided and upfield shifted. However, this peak of LEU was still present in the profile of current LFCs without division or shifting.<sup>25</sup> To strongly support this evidence, additional experiments were performed to determine the amino groups of LFCs using 2,4,6-trinitrobenzenesulfonic acid (TNBS) reactive agent. TNBS is widely used for determining amino acids and peptides and for protein modification.<sup>30,31</sup> Table 4 gives the quantitation of free amine groups of LEU acetate and LFCs. The results indicated that there was no detection of amine groups after incubation with TNBS reagent. Collectively, all the data evidenced that those fatty acids were conjugated with LEU at the Arg residue, not at the His residue.

Structural characterization of LEU acetate and LFCs was confirmed by FT-IR and <sup>1</sup>H-NMR analyses. FT-IR spectra were used to determine the changes in functional groups between the LEU and LFCs (Figure 2). The peak at 1626 cm<sup>-1</sup> indicates the formation of an amide bond between the amino group of LEU and fatty acid. In addition, the LFCs produced a change in the wavenumber. The stretching of a peak of both LPC and LSC at 1690 cm<sup>-1</sup> was longer than in a peak at 1715 cm<sup>-1</sup> as compared to in NHS esters and physical mixtures of LEU and NHS ester of each FA, which attributed to N-H formation after conjugation. Moreover, characteristic absorption peaks at 2850 and 2920 cm<sup>-1</sup> were detected, relating to the -CH<sub>2</sub> groups of the fatty chain length.<sup>22,31</sup>

To identify the fattigation site, the <sup>1</sup>H-NMR spectra of LEU and the three conjugates were identified (Figure 3). The peak at 10.82 ppm in the spectra of LEU was assigned to protons on the imidazole ring.<sup>25</sup> When conjugated to the imidazolyl group, a peak tends to move downfield, but this has not been confirmed.<sup>32</sup> Besides, the 6.76 and 7.50 ppm peaks of LEU were shifted to 7.22 and 7.82 ppm of LFC. This can be presumed to be a change in the protons attached to the guanidine group. In addition, the <sup>1</sup>H-NMR spectra of LEU-fatty acid conjugates showed marked peaks at 1.2–1.3 ppm and at 0.88 ppm, which are related to the (-CH<sub>2</sub>)<sub>n</sub> chain and the CH<sub>3</sub> tail, respectively, from fatty acid conjugation.<sup>31</sup>

The structural modulation of different types of LFCs was identified by MALDI-TOF/TOF analysis (Figure 4). The molecular masses of LEU and LFCs (C12, C16, and C18) were found to be 1209.71 m/z (LEU), 1391.77 m/z (LLC, C12), 1448.00 m/z (LPC, C16), and 1475.95 m/z (LSC, C18). These results are consistent with the calculated ideal values. This indicated that each saturated fatty acid was conjugated with a single LEU molecule.

Lipid conversion of LEU can affect drug release and chemical stability. To investigate this, LFC was characterized using DSC. As a result, a DSC thermogram was conducted to study the effect of treatment methods on the

**Table 4** Quantitation of Free Amine Groups of LEU Acetate and LFCs

Samples	Expected Concentration (mM)	Measured Concentration (mM)
LEU	0.0394	0.0390 $\pm$ 0.0014
LLC	0.0394	No detection
LPC	0.0394	No detection
LSC	0.0394	No detection

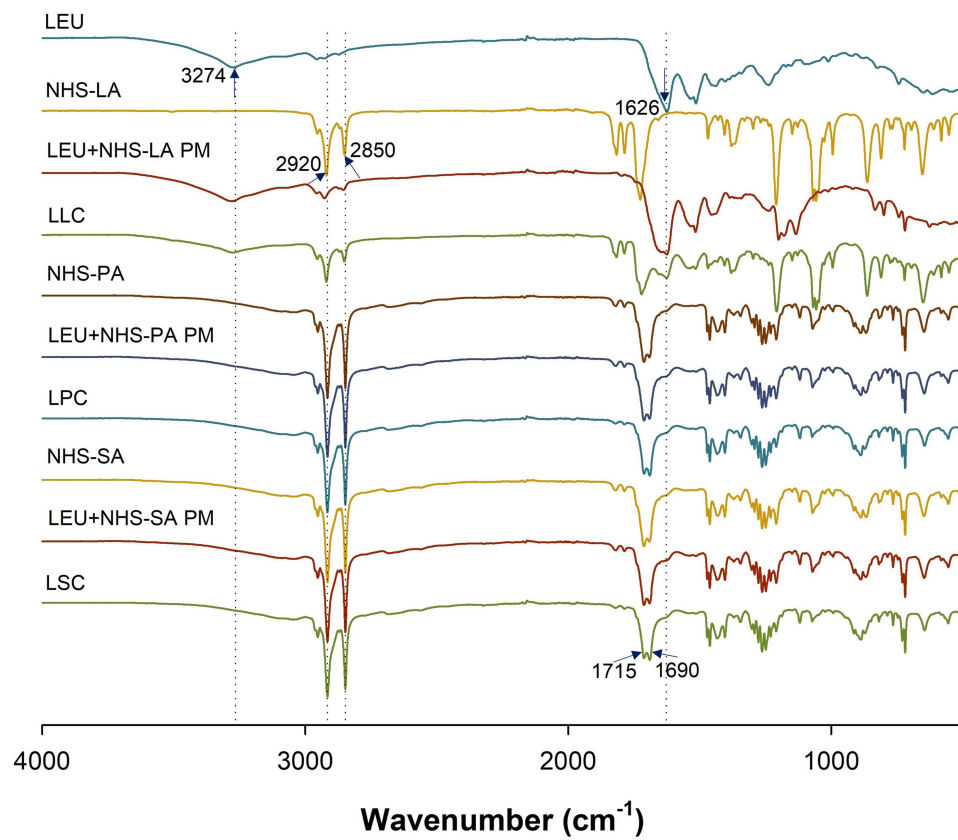


**Figure 2** FT-IR spectra of LEU acetate, NHS-FA esters, physical mixtures of LEU and NHS-FA esters, and three conjugates (LFCs).

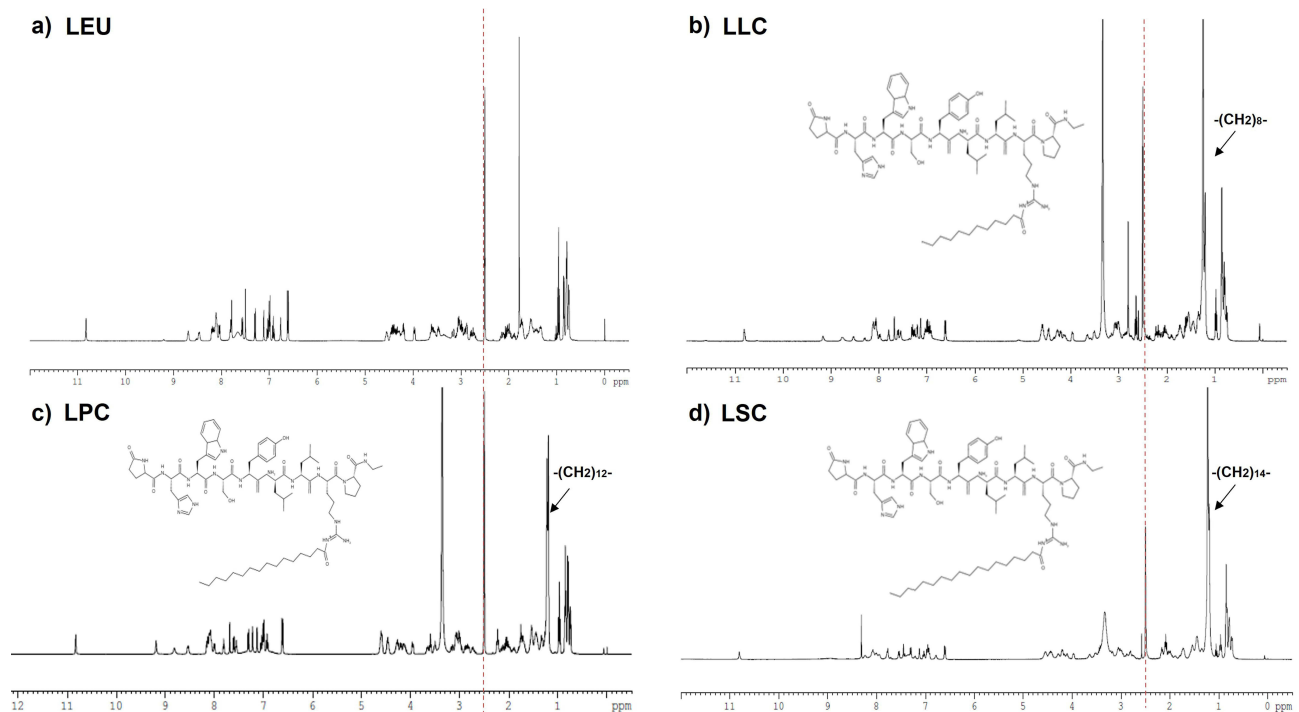


**Figure 3**  $^1\text{H-NMR}$  spectra of (a) LEU acetate, (b) LEU-lauric acid conjugate (LLC), (c) LEU-palmitic acid conjugate (LPC), and (d) LEU-stearic acid conjugate (LSC).

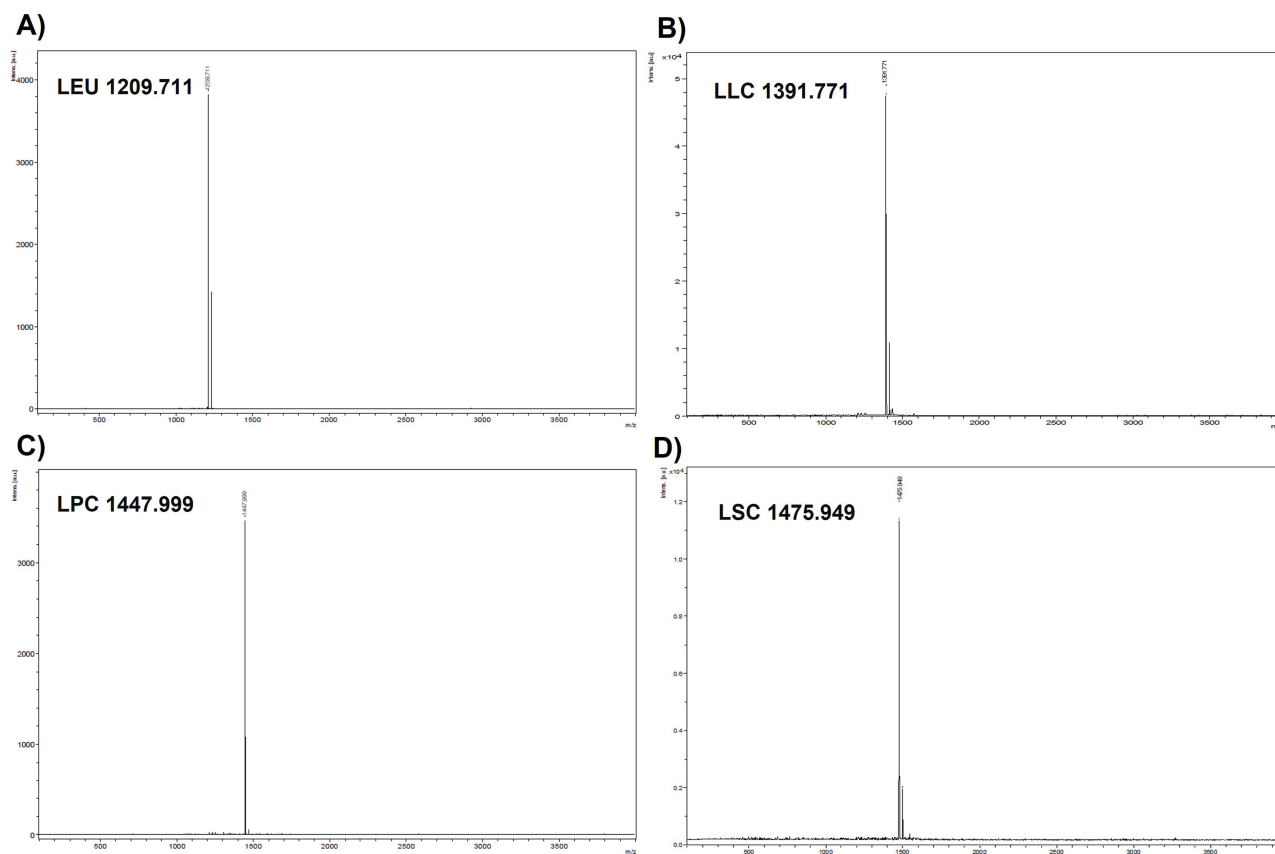


**Figure 4** MALDI-TOF analysis of (A) LEU acetate, (B) LEU-lauric acid conjugate (LLC), (C) LEU-palmitic acid conjugate (LPC), and (D) LEU-stearic acid conjugate (LSC).

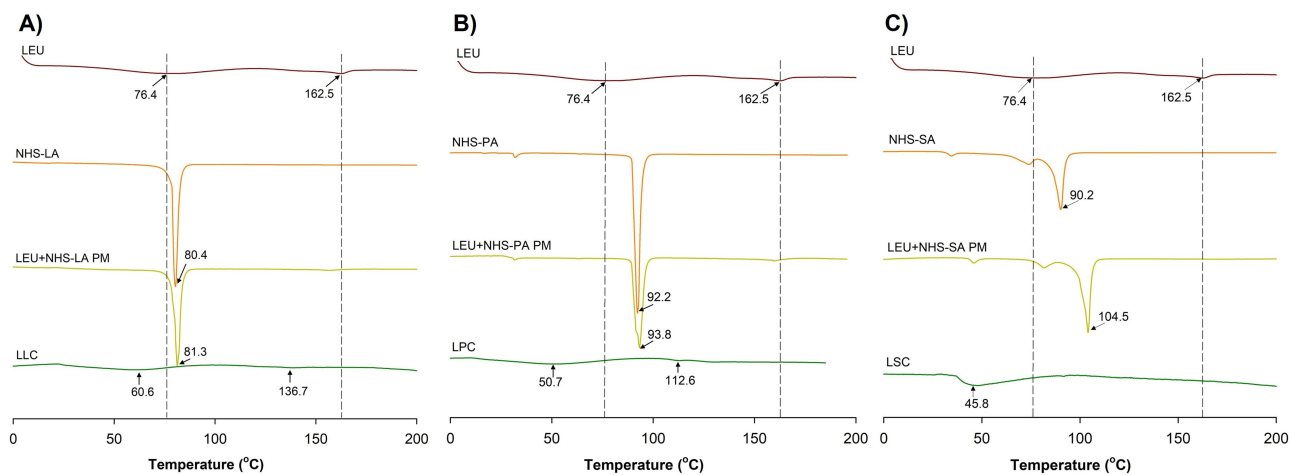


**Figure 5** DSC thermograms of LEU acetate, NHS-FA esters, physical mixtures of LEU and NHS-FA esters, and three conjugates (LFCs). (A) LLC, (B) LPC, and (C) LSC.

crystallinity of pure drug and LFCs. The DSC spectra of the different types of LFCs are shown in Figure 5. Based on the DSC results, various types of NHS-FA esters (NHS-LA, NHS-PA and NHS-SA) had melting peaks at 80.4, 92.2, and 90.2 °C, respectively. In the thermogram of the LFCs, all the peaks disappeared. In addition, in the spectra of all LFCs, two thermal characteristic peaks of LEU positioned at 76.4 and 162.5 °C were shifted into lower



melting points. Interestingly, the longer the chain of fatty acid that was used, the lower the melting point of a conjugate was achieved. Collectively, it appears that the LFCs were in an amorphous state after conjugation.

## Characterization of Self-Assembly of LFCs (LFNs)

To elucidate the secondary structure of the peptide after fatty acid conjugation, CD spectra of LEU and LFCs were performed in water and 50% 2,2,2-trifluoroethanol (TFE) and are shown in Figure 6A and B, respectively. In water solution, LEU and LFCs spectra were depicted with a single large negative peak at around 200 nm, featuring a major random coil structure.<sup>33</sup> In the solution of 50% TFE, three LFCs still performed predominantly random coil structures like that of LEU with a single negative peak at around 203 nm. Herein, the remained unchanged secondary structure of LEU in water and 50% TFE could be affected by the number of amino acids (9 amino acids) contained in the peptide chain, as compared to CM4 (35 amino acids) or CAMEL (15 amino acids) as reported in previous studies.<sup>34,35</sup> Taken together, the CD results indicated that the self-assembled behaviors of three LFCs could be due to the aggregations of hydrophobic tails of fatty acids in conjugates without affecting the secondary structure of LEU in conjugates. The surface morphology of pure LEU and LFCs (C12, C16, and C18) was visualized by FE-SEM, as shown in Figure 6C. Pure LEU was composed of a rectangular shape. The morphology of the LFNs was smooth and spherical. However, in the case of LSC, some large particles were observed irregularly between the small nanoparticles. The shapes of LLN and LPN were more uniform than those of LSN. It is presumed that it was difficult for the fatty acids to form uniformized nanoparticles because of the hydrophobic fatty acid portion. This gives the effect of fatty acid types on the physicochemical properties of self-assembled LFNs according to the hydrophobicity index of fatty acids related to the chain lengths, including particle size. The physicochemical properties of the LFNs, such as particle size, PDI, and zeta potential, were measured by DLS (Table 5). The particle sizes of LLN, LPN, and LSN are  $68.2 \pm 1.8$  nm (PDI  $0.189 \pm 0.012$ ),  $77.4 \pm 2.1$  nm (PDI  $0.174 \pm 0.041$ ), and  $102.0 \pm 4.6$  (PDI  $0.284 \pm 0.034$ ) nm, respectively. The zeta potential values of LLN, LPN, and LSN are  $41.93 \pm 0.67$  mV,  $51.69 \pm 0.39$  mV, and  $66.07 \pm 2.23$  mV, respectively, which indicates the high stability of nanoparticles. Furthermore, more positive nanoparticles were taken up by the cell membrane than neutral or negative nanoparticles. One reason is that both sides of the

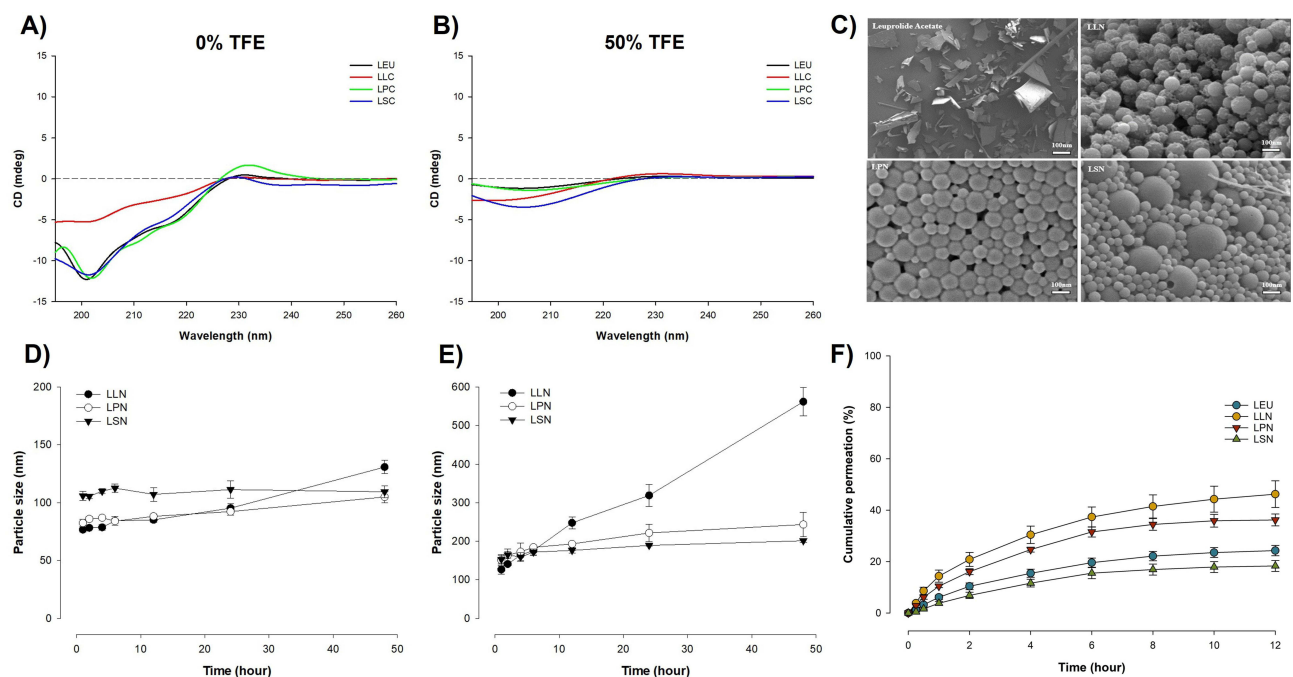


**Figure 6** Self-assembly characterizations of LFCs. (A) and (B) Secondary structure analysis of LEU and LFCs by CD spectroscopy in water and in TFE/water at ratio 50:50 (v/v), respectively. (C) SEM morphology of LEU and three LFNs, (D) short-time stability of LFNs in PBS pH 7.4, (E) short-time stability of LFNs in mimicking physiological condition (5% HSA in PBS pH 7.4), and (F) permeation profiles of LEU and self-assembled LFCs (LFNs) through permeation barrier-membrane (PB-M) using Franz diffusion cells ( $n = 3$ ).

**Table 5** Physicochemical Properties of Self-Assembled LEU-FA Nanoparticles (LFNs)

LFNs	Particle Size (nm)	PDI	Zeta Potential (mV)
LLN (C12)	68.2 ± 1.8	0.189 ± 0.012	41.93 ± 0.67
LPN (C16)	77.4 ± 2.1	0.174 ± 0.041	51.69 ± 0.39
LSN (C18)	102.0 ± 4.6	0.284 ± 0.034	66.07 ± 2.23

membrane surface are negatively charged.<sup>36</sup> Therefore, the electrostatic interactions with negatively charged cell membranes are favorable to entrap the negatively charged nanoparticles.<sup>37</sup>

The short-time stability of three LFNs in pH 7.4 PBS without or with the supplemented human serum albumin (5% w/v HSA) was performed and is illustrated in Figure 6D and E, respectively. In PBS without HSA, there was a slight increase in the particle size of LLN with the shortest chain length of LA conjugated to LEU, while there was no significant difference in the particle size distribution of LSN and LPN after 48 h incubation in PBS. On the other hand, in PBS containing 5% w/v HSA as mimicking a physiological condition, there was an increase in particle size of all LSN after treating with HSA. Herein, the increase in particle size of all LFNs could be the protein corona of the positively charged nanoparticles. Among the three LFNs, LLN showed a faster increase in particle size as compared to LSN and LPN because of the dual impacts of protein corona and low stability in PBS of LLN. Therefore, these results indicated that the chain length of conjugated fatty acids could affect the behaviors of self-assembly of LFCs via the size and stability of nanoparticles (LFNs).

Together with the stability of LFNs, the enhanced permeation of conjugated fatty acids in terms of their carbon chain lengths was investigated using Franz diffusion cells to compare the permeation of free drug and nanoparticles.<sup>38</sup> The data are shown in Figure 6F. To compare the self-assembly behaviors affecting the permeability of each conjugate, the same concentration of LEU and each conjugate (1 mg/mL) was tested in a final volume for permeation study, instead of using the same equivalent LEU concentration. The cumulative permeability rates of LFNs were 46.23 ± 5.22% (LLN, C12), 36.18 ± 2.31% (LPN, C16), and 18.29 ± 2.12% (LSN, C18) until 12 hours. The LLN and LPN permeability rates had greater values of 190.56% and 149.15%, respectively, compared to the same concentration of LEU solution. In contrast, the LSN was inhibited from permeation to 80.13%. This is probably because stearic acid (C18) induces a decrease in the fluidity of the cellulose membrane.<sup>39</sup> This result implied that smaller lipophilic molecules could easily penetrate the passively charged biological membrane.

The self-assembled nanoparticles are beneficial for the enhanced permeability of LEU via the elevated lipophilicity of LFCs. The degradation of LFNs would be slower than in LFCs due to the self-assembled conformation of LFNs, possibly extending the degradation of LEU against peptidases by the disassembly of nanoparticles followed by the hydrolysis of inactive conjugates to convert into active LEU. Taken together, the enhanced permeability of LFCs and self-assembly of LFNs could be beneficial to elevate the enhanced permeability and retention (EPR) effect for progressive accumulation in the tumor.<sup>40</sup>

## Degradation Profiles of LFCs

Prodrugs are pharmacologically inactive or have poor pharmacological activity and should be converted into active drugs in biological environments to elicit the desired pharmacological action. Therefore, the blood stability and conversion of the LFCs prodrug into LEU were determined in human plasma. The stability of LFCs in human plasma was more preferable to rat plasma because of the difference of proteins and enzymes, affecting to the binding capacity (protein corona) of therapeutic agents with plasma proteins.

At first, to confirm the stability of LEU, an *in vitro* dissolution study was carried out under human plasma conditions. Figure 7A shows the *in vitro* degradation profile of LEU in human plasma. The LEU concentration decreased to 58.28 ± 5.88% of LEU over 21 days. In the same way, Figure 7B shows the degradation and conversion profile of LFCs in human plasma, remaining only 5.65 ± 5.30% for LLC (C12) and 8.99 ± 5.92% for LPC (C16) within 21 days, while 10.23 ± 6.21% LSC (C18) within 28 days. The synthesized prodrug was rapidly converted into LEU by the enzyme present in the

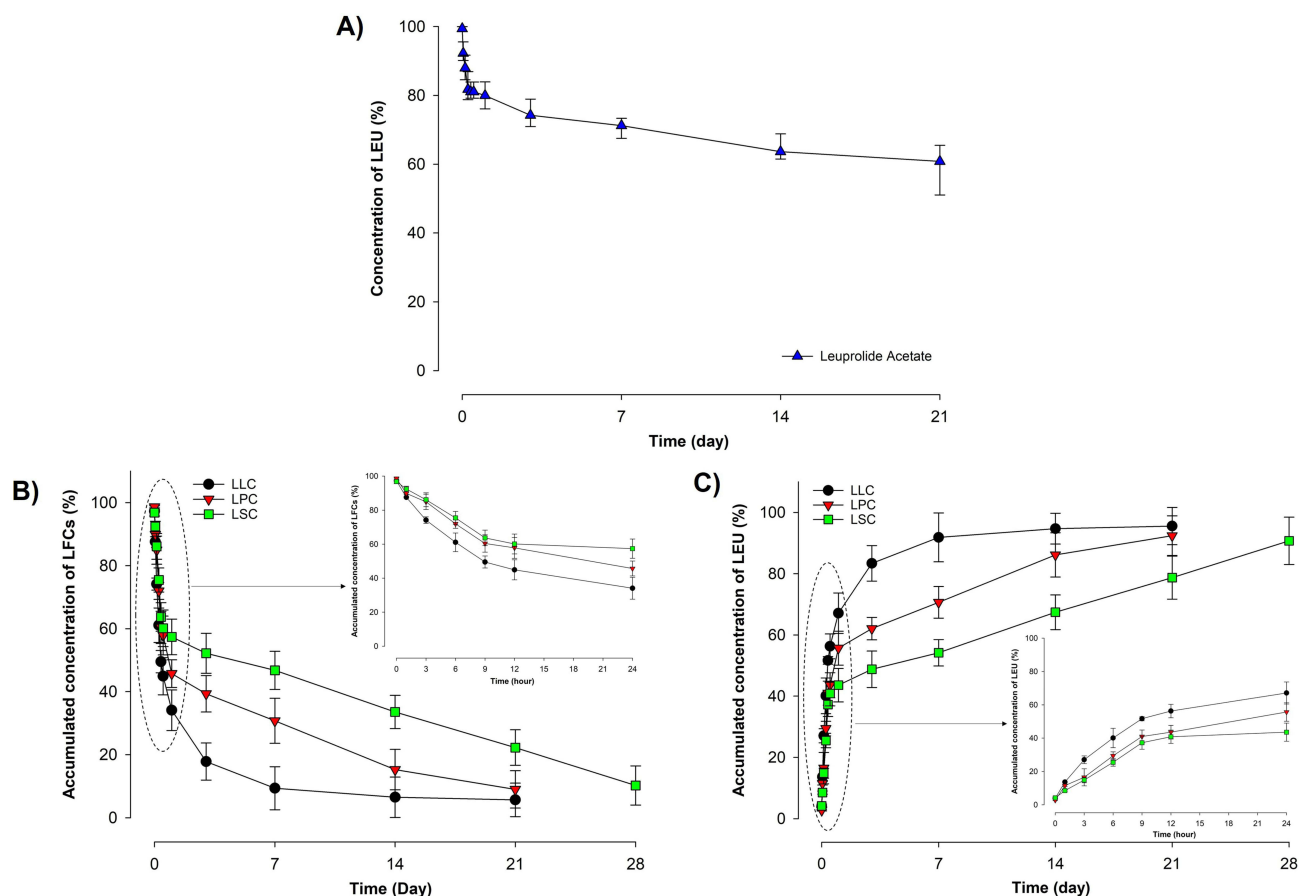


**Figure 7** Degradation profiles in human plasma of (A) LEU, (B) LFCs, and (C) converted LEU concentration from LLC, LPC, and LSC (n = 3).

plasma. The speed of conversion is proportional to the chain length of the fatty acids. LLC (C12) was the least lipophilic and rapidly converted to LEU, with  $95.5 \pm 6.09\%$  within 21 days, showed in **Figure 7C**. With other conjugated lengths of fatty acid conjugation, LPC (C16) and LSC (C18) were converted with  $92.42 \pm 6.47\%$  and  $90.74 \pm 7.74\%$  within 21 and 28 days into active LEU, respectively.

Based on these results, the rate of decay of the prodrug or conversion to LEU was dependent on the chain length of the fatty acids. All LFCs sustained drug release more than LEU alone due to the amphiphilic conjugational modification of chemical structure and self-assembly as illustrated in **Figure 6**. Therefore, the structural modification of peptides and biologicals provides several opportunities for proteolytic stability. The strategy of constructing the amphiphilic conjugational prodrug and its self-assembly can protect the prodrug from degradation by proteases and other enzymes. Correspondingly, the fabrication of conjugated peptide drugs with fatty acids could be a challenging method to extend the degradation of the half-life and control the biopharmaceutical druggability of an LEU peptide. It is worth mentioning that LEU conjugation with fatty acids protects the LEU against enzymatic degradation. This enhancement could be the potential to prolong the direct inhibitory activity of LEU for cancer treatment.<sup>25,28</sup>

## Cytotoxicity of LFCs Against Cancer and Non-Cancerous Cell Lines

The cytotoxicity of LFCs was evaluated in both cancer cells and non-cancerous cell lines to determine the selectivity index (SI) of each conjugate. As shown in **Figure 8**, the anticancer effect of all LFCs was significantly higher than the parent LEU. The concentration of LFCs above  $50 \mu\text{M}$  was considered to exhibit cytotoxicity to all cell lines with a significant reduction of cell viability. Interestingly, there was chain length-dependent cytotoxicity against cancer cells and non-cancerous cells in this study. In both normal cell lines, the shorter chain length in LLC and LPC exerted higher toxicity as compared to the highest chain length of LSC. This trend was contrary to the performance of LFCs in cancer

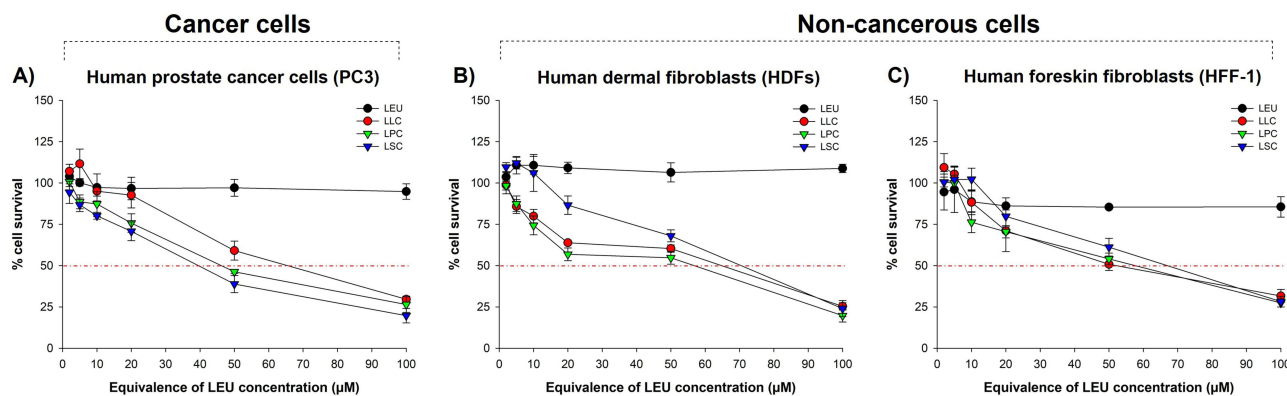


**Figure 8** Cytotoxicity of LFCs against cancer cells and non-cancerous cell lines after 24 h of incubation by WST-1 assay. **(A)** Human prostate cancer cells (PC3), **(B)** human dermal fibroblasts (HDFs), and **(C)** human foreskin fibroblasts (HFF-1).

cells. Among three LFCs, as calculated in Table 6, only LSC obtained the selectivity index value above 2 in both normal cell lines, revealing the potential cancer targeting of LSC. The differences in selective toxicity to cancer cells over normal cells among three LFCs could be explained by the self-assembly behaviors of LFCs and many differences in the expression of receptors among these cell lines. In cancer cells, PC3 are well known as lipid-dependent cells, and mainly utilize FAs from the external environment as energy for cell growth.<sup>23</sup> Therefore, the overexpression of free fatty receptors (FFARs) or CD36 membrane protein for the uptake of long-chain FAs extensively pronounced in previous studies for the PC3 cell line could be advantageous for the higher uptake of LSC as compared to LLC.<sup>41</sup> On the other hand, the lower expression of FA receptors could reduce the active transport of LFCs through the cell membrane of normal cells; thereby the cytotoxicity against normal cell lines could be explained through the self-assembled behaviors of LFCs. As mentioned in the characterization of LFNs, LLN with the smallest particle size and the enhanced permeability could easily enter intracellular space throughout the passive transport mechanism, as compared to LSN with the larger size and the lower permeability. Therefore, the treatment of LSC caused less cytotoxicity toward normal cell lines compared to LLC.

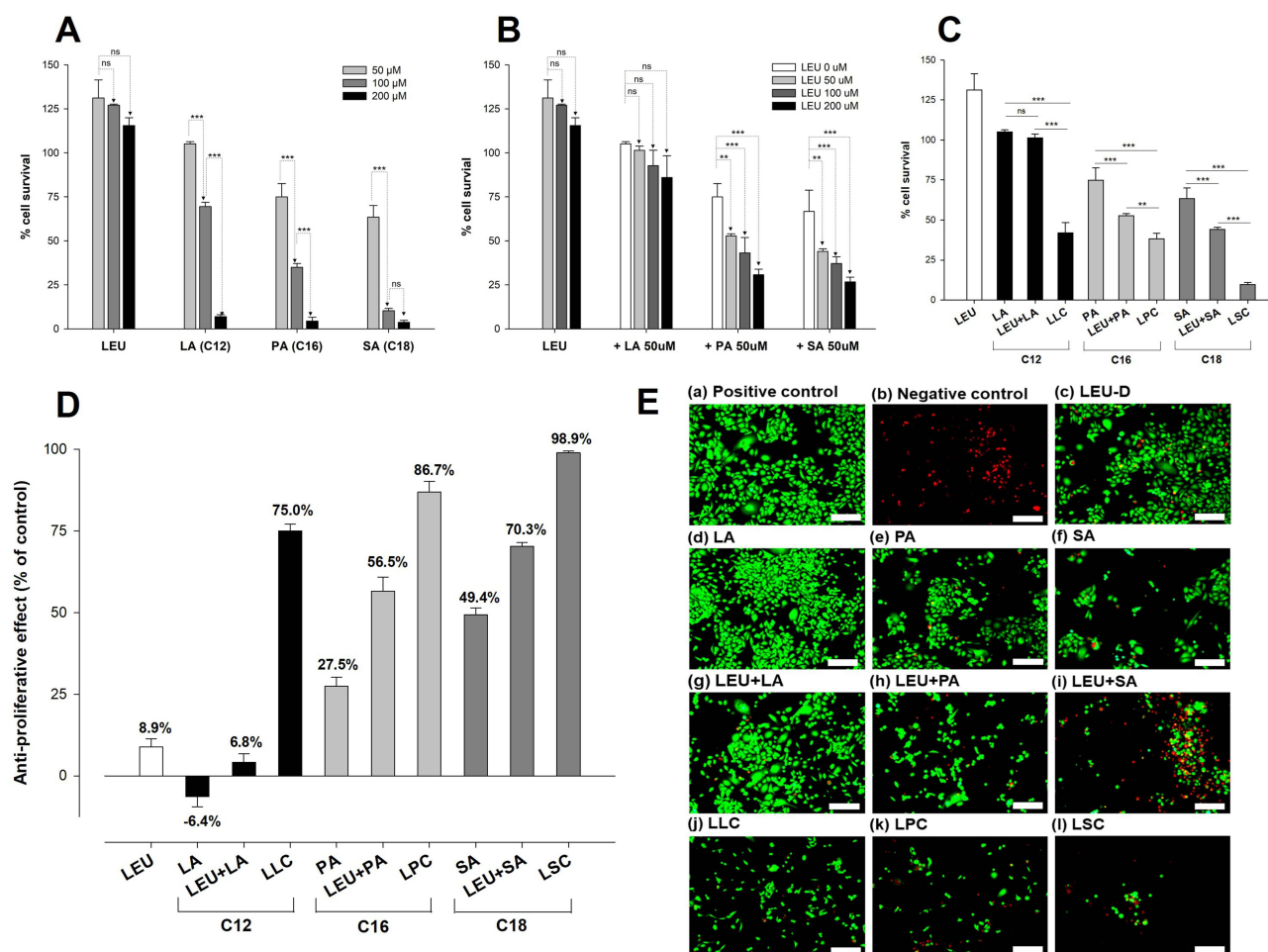
### AntiProliferative Effects of LFCs on 2D Monolayer Culture Model

Figure 9A shows the effects of the one-time treatment of LEU and three types of free FAs on the proliferation of PC3 cells after 72 h incubation. Obviously, the increase of LEU concentration from 50 to 200 μM slightly inhibited the cell growth but with no significant statistical difference. In addition, this inhibition of cell growth was inferior to the control sample, which was higher than 100% of cell survival in all treated concentrations of LEU. This phenomenon could be from the limited stability of LEU in serum.<sup>12</sup> On the other hand, three free FAs performed their superior effects on the antiproliferation of cancer cells, even at the smallest treated concentration (50 μM) as compared to in LEU. Among the

**Table 6** The IC<sub>50</sub> and SI Values of LFCs in Cancer and Non-Cancerous Cells

LFCs	Cancer Cells		Non-Cancerous Cells			
	PC3		HDFs		HFF-1	
	IC <sub>50</sub> (μM)		IC <sub>50</sub> (μM)	SI	IC <sub>50</sub> (μM)	SI
LLC	78.7 ± 10.6		45.9 ± 4.9	0.6	56.7 ± 16.4	0.7
LPC	47.6 ± 6.3		35.8 ± 4.8	0.8	48.7 ± 7.1	1.0
LSC	35.4 ± 1.1		82.4 ± 10.0	2.3	70.7 ± 9.0	2.0

**Notes:** The IC<sub>50</sub> is defined as the concentration of experimental sample corresponds to a 50% of cell growth inhibition. The selectivity index (SI) was calculated for each conjugate following the formula: SI = IC<sub>50</sub> of non-cancerous cell line / IC<sub>50</sub> of cancer cell line.



**Figure 9** Antiproliferative effect in 2D monolayer culture. **(A)** Cell proliferation after the treatment of LEU and three FAs at three concentrations (50, 100, 200  $\mu$ M) after 72 h. **(B)** Cell proliferation after the treatment of three FAs at 50  $\mu$ M with different concentration of LEU (50, 100, 200  $\mu$ M) after 72 h. **(C)** Cell proliferation after the treatment of three FAs, three LFCs and physical mixtures of LEU and FAs at 50  $\mu$ M after 72h. **(D)** Inhibition of cell proliferation after the treatment of LEU and three LFCs repeated daily at a dose of 50  $\mu$ M for 4 days. **(E)** Live/dead images of cell proliferation after the treatment of LEU and three LFCs repeated daily at dose of 50  $\mu$ M for 4 days (scale bar: 250  $\mu$ m) (n = 3). \*\*\*p < 0.001, \*\*p < 0.01, analyzed by one-way ANOVA test.

**Abbreviation:** ns, no significance.

three FAs, SA with the longest chain length significantly inhibited cell growth. In agreement with our previous studies, the chain length of FAs plays a vital role in modulating the cytotoxicity of cancer cells and the long-chain fatty acid, C18 exhibited significant performance to overexpressed free fatty acid receptors (FFARs) on cancer cells.<sup>20,22,42</sup> To overcome the shortcomings of LEU due to the stability issue, we continued studying the combination of LEU and free FAs at 50  $\mu$ M in physical mixtures as illustrated in Figure 9B. Interestingly, the combination of longer chain of FAs (PA and SA) and LEU enhanced the antiproliferative effect on cancer cells as compared to LEU alone or free FAs alone, while the performance with shorter chain length, LA (C12), did not show the effect on cellular cytotoxicity. Herein, we assumed that FAs can increase the stability of LEU in serum via the formation of complexation between the carboxylic group of FA and the amine group of LEU.<sup>43</sup> Next, we performed the proliferation assay with a one-time and same dose (50  $\mu$ M) treatment of different samples, including LEU, free FAs, mixtures of LEU and FAs and three conjugates (LFCs), shown in Figure 9C. The treatment of the shortest chain length (C12) alone or in the combination of LEU at the dose of 50  $\mu$ M did not exert a significant inhibition of cell growth after 3 days as compared to that of its conjugate (LLC). Notably, all three LFCs showed a superior and synergistic inhibitory effect on cell growth as compared to other samples due to the slow degradation of LFCs in serum mentioned in the previous degradation study. Furthermore, the enhanced



permeability of LFCs via the increased lipophilicity and self-assembly by modification with fatty acids could improve the cell-penetrating activity of LFCs.<sup>34</sup>

To further confirm the direct antiproliferation effect of LEU in an androgen-independent cell line, we performed a daily treatment of LEU for 4 days at the same dose of 50  $\mu\text{M}$  with other tested samples.<sup>28</sup> The results are shown in Figure 9D and E. Quantitatively, in this study, LEU showed its ability in antiproliferation of cancer cells with 8.9% of inhibition effect, which is significantly enhanced as compared to previous cell culture studies by one-time treatment. In contrast, the daily treatment of shortest chain length FA (C12) alone or with combined LEU did not perform well the same as in LEU alone and in other longer chain lengths (C16 and C18). In previous research, Vanacker et al investigated the effects of different FAs including LA, PA and SA on the proliferation of peripheral blood mononuclear cells (PBMC) and indicated that all tested fatty acids, excluding lauric acid, significantly reduced the proliferation of cells in a dose-dependent manner.<sup>44</sup> Among three LFCs, LSC with the longest chain length of conjugated FA (C18) exhibited a significant antiproliferative effect with only 1.1% of cell survival (compared to control) after 4 days of treatment.

Figure 9E performed the fluorescence images of a live/dead assay of PC3 cells treated samples after 4 days of incubation. The presence of live cells (green color) was proportional to the data quantified in Figure 9D. Three conjugates showed the sparse intensity of live cells as compared to each component treated in the formulation.

## Anti-Tumor Effects of LFCs in 3D Spheroid Culture Model

The 3D spheroid culture model assay is executed to analyze the therapeutic effect and tumor-penetrating capacity of anticancer therapeutics. A previous report by Kimlin et al indicated that 3D spheroid culture obtains various in vivo characteristics of a solid tumor such as invasion, angiogenesis, metastasis, tumor microenvironment, and drug penetration.<sup>45</sup> As illustrated by the improved inhibition outcomes in previous 2D monolayer cultures, we continued investigating the anti-tumor effects of three conjugates and LEU at the concentration of 50  $\mu\text{M}$  with a one-time treatment as compared to daily treatment of LEU-D for 7 days throughout the observation of spheroid morphology and size shown in Figure 10. The control and LEU samples showed the expansion of spheroid volume after day 3 and cells started to invade the spheroid body, showing the metastatic potential in cancer development.<sup>46</sup> In contrast, the treatment of three conjugates and daily LEU, LEU-D, exerted the inhibition of cells invaded from the spheroid body. However, the treatment of the spheroid by LEU-D did not reduce of growth of spheroid volume as compared to the control and LEU samples, as quantified in Figure 10B. On the other hand, three conjugates showed the inhibition of tumor growth by slowing down the increase of spheroid volume as in the control, LEU, and LEU-D samples. Moreover, three conjugates exerted a superior effect in killing cells inside the spheroid body, while the treatment of LEU-D enhanced the killing effect on the edge of the spheroid. The enhanced anti-tumor effect observed in Figure 10A and B could be from the improved serum stability and permeability of three conjugates as compared to LEU. In addition, the importance of the fatty chain length in conjugate also supported the anticancer activity of LEU via the overexpression of FFARs on the cancer cells.<sup>22</sup> Therefore, among three LFCs, LSC with the longest fatty chain length performed the clearest effects on inhibitory cancer growth with a significantly reduced spheroid volume (\*\* $p < 0.01$ ) and no cell invasion. Herein, we found that LEU could show its direct inhibitory effect on cell growth if we performed the daily treatment during culture, which illustrates the limitation of LEU with low stability in serum. By conjugating with FAs, LFCs enhance the anti-tumor effect of LEU by increasing the stability of LEU and strengthening the direct inhibitory effect of LEU.

## Conclusions

Guanidine-targeted conjugates of LEU with different chain lengths of fatty acids, including lauric, palmitic, and stearic acids, were successfully synthesized. Different chain lengths of fatty acids affected the physicochemical properties of conjugates in terms of degradation rate, self-assembly behaviors, and peptide permeation. By conjugation with fatty acids, the stability of LEU in human plasma/serum was significantly improved throughout the self-assembled behaviors together with the slow degradation rate. Furthermore, different chain lengths of saturated fatty acids could provide versatility to synthesize LEU conjugates to form LFNs for enhanced peptide permeability. More importantly, our research indicated that conjugation of different chain lengths of fatty acids not only enhanced the physicochemical properties of LEU, but also effectively improved the anticancer activity of LEU by exerting a superior direct inhibitory effect on the growth of prostate cancer cells and tumors in 2D monolayer and 3D spheroid cell culture studies. Among three chain



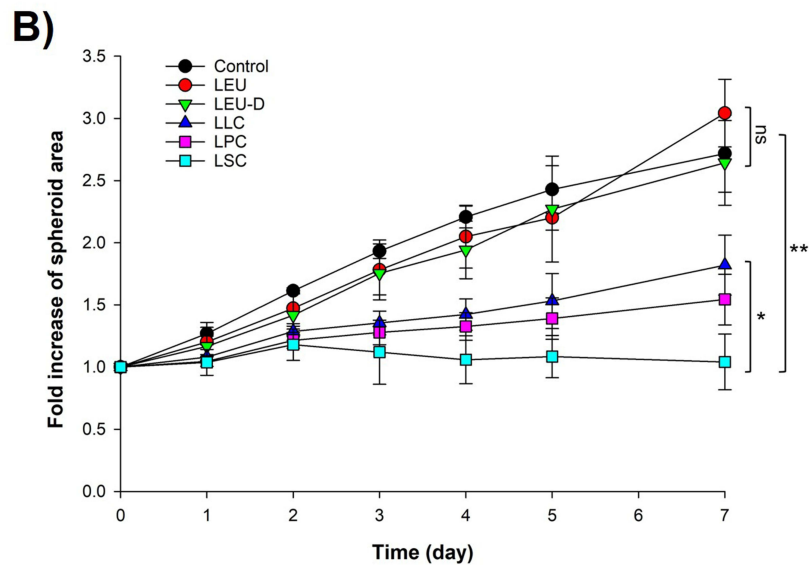
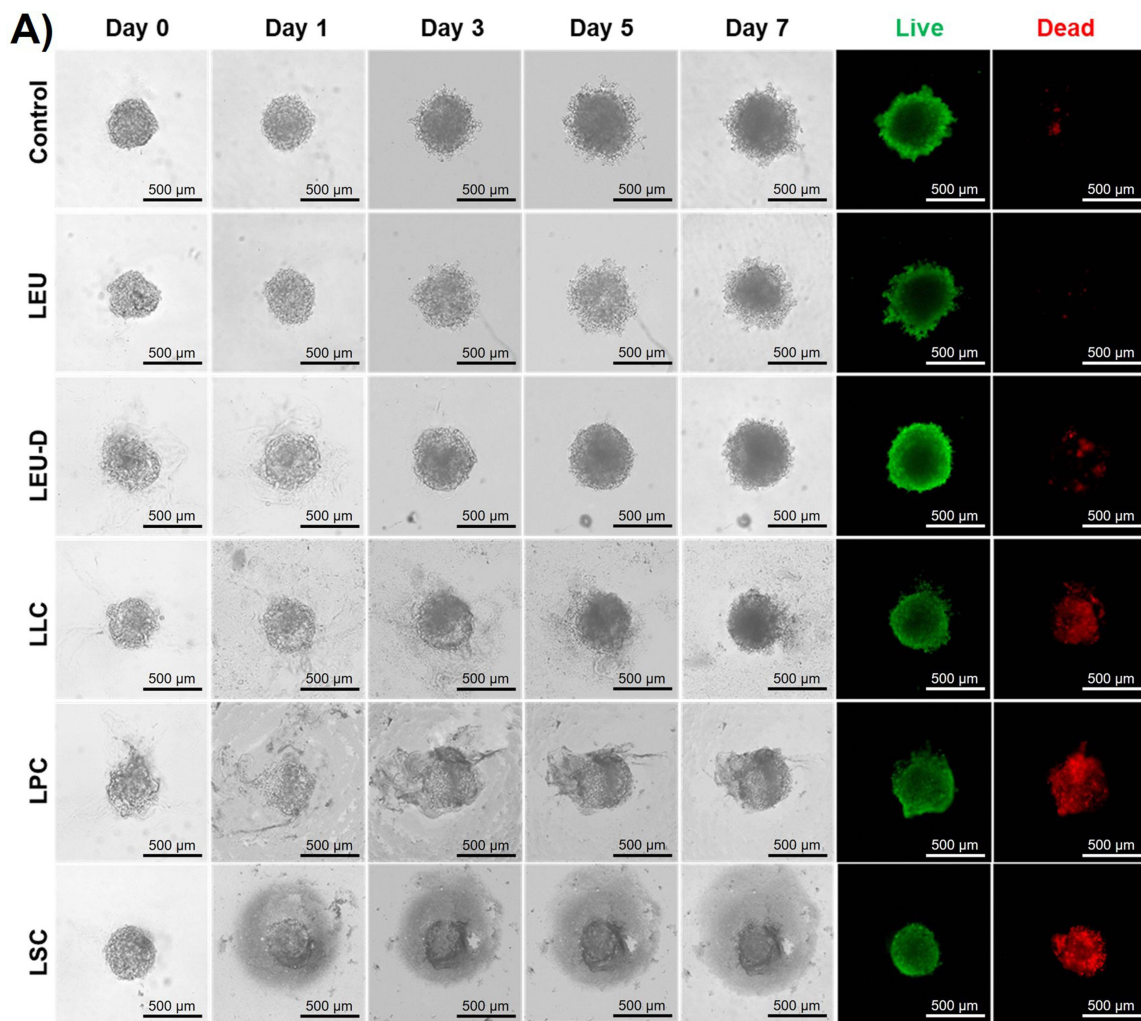


**Figure 10** Anti-tumor effect in 3D spheroid culture. **(A)** Observation of 3D spheroid cultures of PC3 treated with LEU, LEU-D, and three LFCs for 7 days. **(B)** Fold increase of spheroid area after treatment of LEU, LEU-D, and three LFCs for 7 days ( $n = 3$ ).  $**p < 0.01$ ,  $*p < 0.05$ , analyzed by one-way ANOVA test. **Abbreviation:** ns, no significance.

lengths of conjugated FAs, LSC with the longest chain length showed its balance between efficiency and selectivity for cancer targeting with the highest antiproliferative effect in the PC3 cell line and lower cytotoxicity against normal cell lines. Taken together, this finding appears to be more effective and potential for improving anticancer activity against several hormone-responsive tumor systems using therapeutic peptides, especially for some cancer models that are resistant to hormone therapy by exerting an additional superior direct inhibitory effect with conjugated long-chain fatty acids.

## Abbreviations

LEU, Leuprolide; LFC, Leuprolide–fatty acid conjugate; LLC, Leuprolide–lauric acid conjugate; LPC, Leuprolide–palmitic acid conjugate; LSC, Leuprolide–stearic acid conjugate; LFN, Leuprolide–fatty acid nanoparticle; LLN, Leuprolide–lauric acid nanoparticle; LPN, Leuprolide–palmitic acid nanoparticle; LSN, Leuprolide–stearic acid nanoparticle; FT-IR, Fourier transform-infrared spectroscopy; DSC, Differential scanning calorimetry; DLS, Dynamic light scattering; FE-SEM, Field emission scanning electron microscope; HPLC, High-performance liquid chromatography.

## Data Sharing Statement

The data presented in this study are available upon request.

## Acknowledgments

This work was supported by a grant from the National Research Foundation of Korea (NRF) funded by the Ministry of Science and ICT (2020R1A2C2008307) and the Korea Evaluation Institute of Industrial Technology (KEIT) funded by the Ministry of Trade, Industry, and Energy (20008840), Republic of Korea. We would like to thank the staff of Ajou Central Laboratory for allowing us to use the field emission-scanning electron microscopy (FE-SEM), differential scanning calorimetry (DSC), and Fourier-transform infrared (FT-IR) spectroscopy facilities. Last but not least, we sincerely thank Ms. Thanh-Hang Ngo at Molecular Science and Technology Research Center (MSTRC, Ajou University) who enthusiastically advised us to execute the 3D spheroid culture study.

## Disclosure

The authors declare that they have no known competing financial interests or personal relationships that could have influenced the work reported in this paper.

## References

1. Greenlee RT, Hill-Harmon MB, Murray T, Thun M. Cancer statistics, 2001. *CA Cancer J Clin*. 2001;51(1):15–36. doi:10.3322/canjclin.51.1.15
2. Litwin MS, Tan H-J. The diagnosis and treatment of prostate cancer: a review. *JAMA*. 2017;317(24):2532–2542. doi:10.1001/jama.2017.7248
3. Sumanasuriya S, De Bono J. Treatment of advanced prostate cancer—A review of current therapies and future promise. *Cold Spring Harb Perspect Med*. 2018;8(6):a030635. doi:10.1101/cshperspect.a030635
4. Raghavan D. First-line use of novel hormonal agents in prostate cancer: a critical appraisal. *Clin Adv Hematol Oncol*. 2018;16(4):289–295.
5. Ceresoli G, De Vincenzo F, Sauta M, Bonomi M, Zucali P. Role of chemotherapy in combination with hormonal therapy in first-line treatment of metastatic hormone-sensitive prostate cancer. *Q J Nucl Med Mol Imaging*. 2015;59(4):374–380.
6. Wilson AC, Vadakkadath Meethal S, Bowen RL, Atwood CS. Leuprolide acetate: a drug of diverse clinical applications. *Expert Opin Investig Drugs*. 2007;16(11):1851–1863. doi:10.1517/13543784.16.11.1851
7. Wu C, Luo X, Baldursdottir SG, Yang M, Sun X, Mu H. In vivo evaluation of solid lipid microparticles and hybrid polymer-lipid microparticles for sustained delivery of leuprolide. *Eur J Pharm Biopharm*. 2019;142:315–321. doi:10.1016/j.ejpb.2019.07.010
8. Kim Y-C, Min KA, Jang D-J, et al. Practical approaches on the long-acting injections. *J Pharm Investig*. 2020;50(2):147–157. doi:10.1007/s40005-019-00452-0
9. Satapathy SR, Sahoo RN, Satapathy B, Immani R, Panigrahi L, Mallick S. Development and characterization of leuprolide acetate encapsulated PLGA microspheres for parenteral controlled release depot injection. *Indian J Pharm Educ Res*. 2021;55:107–116. doi:10.5530/ijper.55.1.14
10. Enayati M, Mobeidi H, Hojjati-Emami S, Mirzadeh H, Jafari-Nodoushan M. In situ forming PLGA implant for 90 days controlled release of leuprolide acetate for treatment of prostate cancer. *Polym Adv Technol*. 2017;28(7):867–875. doi:10.1002/pat.3991
11. Bhatia S. leuprolide injection: implications for monitoring therapy. *Pediatrics Electronic Pages [serial online]* 109. *Inpharma*. 2002;1329:16.
12. Montagnani Marelli M, Moretti RM, Mai S, Procacci P, Limonta P. Gonadotropin-releasing hormone agonists reduce the migratory and the invasive behavior of androgen-independent prostate cancer cells by interfering with the activity of IGF-I. *Int J Oncol*. 2007;30(1):261–271.
13. Dondi D, Limonta P, Moretti RM, Marelli MM, Garattini E, Motta M. Antiproliferative effects of luteinizing hormone-releasing hormone (LHRH) agonists on human androgen-independent prostate cancer cell line DU 145: evidence for an autocrine-inhibitory LHRH loop. *Cancer Res*. 1994;54(15):4091–4095.

14. Loop SM, Gorder CA, Lewis SM, Sainers JH, Drivdahl RH, Ostenson RC. Growth inhibition of human prostate tumor cells by an agonist of gonadotrophin-releasing hormone. *Prostate*. 1995;26(4):179–188. doi:10.1002/pros.2990260403
15. Connor JP, Buller RE, Conn PM. Effects of GnRH analogs on six ovarian cancer cell lines in culture. *Gynecol Oncol*. 1994;54(1):80–86. doi:10.1006/gyno.1994.1170
16. Kowalczyk R, Harris PW, Williams GM, Yang S-H, Brimble MA. Peptide lipidation—a synthetic strategy to afford peptide based therapeutics. *Peptides Peptide Based Biomat Biomed Appl*. 2017;2017:185–227.
17. Hutchinson JA, Burholt S, Hamley IW, et al. The effect of lipidation on the self-assembly of the gut-derived peptide hormone PYY3–36. *Bioconj Chem*. 2018;29(7):2296–2308. doi:10.1021/acs.bioconjchem.8b00286
18. Meghani NM, Amin HH, Tran TT, Tran PH, Park C, Lee B-J. Modulation of serum albumin protein Corona for exploring cellular behaviors of fattigation-platform nanoparticles. *Colloids Surf B Biointerfaces*. 2018;170:179–186. doi:10.1016/j.colsurfb.2018.05.060
19. Park J, Ngo HV, Jin H-E, Lee KW, Lee B-J. Hydroxyl group-targeted conjugate and its self-assembled nanoparticle of peptide drug: effect of degree of saturation of fatty acids and modification of physicochemical properties. *Int J Nanomedicine*. 2022;17:2243. doi:10.2147/IJN.S356804
20. Park C, Meghani N, Amin H, et al. The roles of short and long chain fatty acids on physicochemical properties and improved cancer targeting of albumin-based fattigation-platform nanoparticles containing doxorubicin. *Int J Pharm*. 2019;564:124–135. doi:10.1016/j.ijpharm.2019.04.038
21. Park C, Meghani N, Loebenberg R, Cui J-H, Cao Q-R, Lee B-J. Fatty acid chain length impacts nanonizing capacity of albumin-fatty acid nanomicelles: enhanced physicochemical property and cellular delivery of poorly water-soluble drug. *Eur J Pharm Biopharm*. 2020;152:257–269. doi:10.1016/j.ejpb.2020.05.011
22. Park C, Baek N, Loebenberg R, Lee B-J. Importance of the fatty acid chain length on in vitro and in vivo anticancer activity of fattigation-platform albumin nanoparticles in human colorectal cancer xenograft mice model. *J Control Release*. 2020;324:55–68. doi:10.1016/j.jconrel.2020.05.001
23. Chrzanoska A, Olejarz W, Kubiak-Tomaszewska G, Ciechanowicz AK, Struga M. The effect of fatty acids on ciprofloxacin cytotoxic activity in prostate cancer cell lines—does lipid component enhance anticancer ciprofloxacin potential? *Cancers*. 2022;14(2):409. doi:10.3390/cancers14020409
24. Zhao J, Zhi Z, Wang C, et al. Exogenous lipids promote the growth of breast cancer cells via CD36. *Oncol Rep*. 2017;38(4):2105–2115. doi:10.3892/or.2017.5864
25. Fu M, Zhuang X, Zhang T, Guan Y, Meng Q, Zhang Y. PEGylated leuprolide with improved pharmacokinetic properties. *Bioorg Med Chem*. 2020;28(4):115306. doi:10.1016/j.bmc.2020.115306
26. Grundler V, Gademann K. Direct arginine modification in native peptides and application to chemical probe development. *ACS Med Chem Lett*. 2014;5(12):1290–1295. doi:10.1021/ml5003508
27. Van Ngo H, Park C, Tran TT, Lee B-J. Mechanistic understanding of salt-induced drug encapsulation in nanosuspension via acid-base neutralization as a nanonization platform technology to enhance dissolution rate of pH-dependent poorly water-soluble drugs. *Eur J Pharm Biopharm*. 2020;154:8–17. doi:10.1016/j.ejpb.2020.07.001
28. Pappa EV, Zompra AA, Spyrianti Z, et al. Enzymatic stability, solution structure, and antiproliferative effect on prostate cancer cells of leuprolide and new gonadotropin-releasing hormone peptide analogs. *Peptide Sci*. 2011;96(3):260–272. doi:10.1002/bip.21521
29. Samoto M, Matsuyama H, Matsumoto H, et al. Novel bone microenvironment model of castration-resistant prostate cancer with chitosan fiber matrix and osteoblasts. *Oncol Lett*. 2021;22(4):1–11. doi:10.3892/ol.2021.12950
30. Park C, Vo CL-N, Kang T, Oh E, Lee B-J. New method and characterization of self-assembled gelatin–oleic nanoparticles using a desolvation method via carbodiimide/N-hydroxysuccinimide (EDC/NHS) reaction. *Eur J Pharm Biopharm*. 2015;89:365–373. doi:10.1016/j.ejpb.2014.12.002
31. Tran PH-L, Tran TT-D, Vo TV, Vo CL-N, Lee B-J. Novel multifunctional biocompatible gelatin-oleic acid conjugate: self-assembled nanoparticles for drug delivery. *J Biomed Nanotechnol*. 2013;9(8):1416–1431. doi:10.1166/jbn.2013.1621
32. Boyer C, Liu J, Wong L, Tippett M, Bulmus V, Davis TP. Stability and utility of pyridyl disulfide functionality in RAFT and conventional radical polymerizations. *J Polym Sci a Polym Chem*. 2008;46(21):7207–7224. doi:10.1002/pola.23028
33. Fu M, Zhuang X, Zhang T, Guan Y, Meng Q, Zhang Y. Hydrogen-bonded films for zero-order release of leuprolide. *Macromol Biosci*. 2020;20(9):2000050. doi:10.1002/mabi.202000050
34. Ma L, Huang S, Xie H, et al. Influence of chain length on the anticancer activity of the antimicrobial peptide CAMEL with fatty acid modification. *Eur J Med Chem*. 2022;239:114557. doi:10.1016/j.ejmech.2022.114557
35. Yang Y, Zhang H, Wanyan Y, et al. Effect of hydrophobicity on the anticancer activity of fatty-acyl-conjugated CM4 in breast cancer cells. *ACS omega*. 2020;5(34):21513–21523. doi:10.1021/acsomega.0c02093
36. Pekker M, Shneider M. Interaction between electrolyte ions and the surface of a cell lipid membrane. *J Phys Chem Biophys*. 2015;5(2):2161–2398.
37. Forest V, Pourchez J. Preferential binding of positive nanoparticles on cell membranes is due to electrostatic interactions: a too simplistic explanation that does not take into account the nanoparticle protein Corona. *Mater Sci Eng C*. 2017;70:889–896. doi:10.1016/j.msec.2016.09.016
38. Alves AC, Ramos II, Nunes C, et al. On-line automated evaluation of lipid nanoparticles transdermal permeation using Franz diffusion cell and low-pressure chromatography. *Talanta*. 2016;146:369–374. doi:10.1016/j.talanta.2015.08.070
39. Chede LS, Wagner BA, Buettner GR, Donovan MD. Electron spin resonance evaluation of buccal membrane fluidity alterations by sodium caprylate and L-menthol. *Int J Mol Sci*. 2021;22(19):10708. doi:10.3390/ijms221910708
40. Wu J. The enhanced permeability and retention (EPR) effect: the significance of the concept and methods to enhance its application. *J Pers Med*. 2021;11(8):771. doi:10.3390/jpm11080771
41. Watt MJ, Clark AK, Selth LA, et al. Suppressing fatty acid uptake has therapeutic effects in preclinical models of prostate cancer. *Sci Transl Med*. 2019;11(478):eaau5758. doi:10.1126/scitranslmed.aau5758
42. Liu Z, Hopkins MM, Zhang Z, et al. Omega-3 fatty acids and other FFA4 agonists inhibit growth factor signaling in human prostate cancer cells. *J Pharmacol Exp Ther*. 2015;352(2):380–394. doi:10.1124/jpet.114.218974
43. Yoo HS, Choi HK, Park TG. Protein–fatty acid complex for enhanced loading and stability within biodegradable nanoparticles. *J Pharm Sci*. 2001;90(2):194–201. doi:10.1002/1520-6017(200102)90:2<194::AID-JPS10>3.0.CO;2-Q
44. Vanacker N, Blouin R, Ster C, Lacasse P. Effect of different fatty acids on the proliferation and cytokine production of dairy cow peripheral blood mononuclear cells. *J Dairy Sci*. 2022;105(4):3508–3517. doi:10.3168/jds.2021-21296
45. Kimlin LC, Casagrande G, Virador VM. In vitro three-dimensional (3D) models in cancer research: an update. *Mol Carcinog*. 2013;52(3):167–182. doi:10.1002/mc.21844
46. Berens EB, Holy JM, Riegel AT, Wellstein A. A cancer cell spheroid assay to assess invasion in a 3D setting. *JoVE*. 2015;105:e53409.

International Journal of Nanomedicine

Dovepress

## Publish your work in this journal

The International Journal of Nanomedicine is an international, peer-reviewed journal focusing on the application of nanotechnology in diagnostics, therapeutics, and drug delivery systems throughout the biomedical field. This journal is indexed on PubMed Central, MedLine, CAS, SciSearch<sup>®</sup>, Current Contents<sup>®</sup>/Clinical Medicine, Journal Citation Reports/Science Edition, EMBase, Scopus and the Elsevier Bibliographic databases. The manuscript management system is completely online and includes a very quick and fair peer-review system, which is all easy to use. Visit <http://www.dovepress.com/testimonials.php> to read real quotes from published authors.

Submit your manuscript here: <https://www.dovepress.com/international-journal-of-nanomedicine-journal>